

Impurity levels, impurity bands, excited impurity bands, and band tails: The electronic density of states in quantum wells and heterostructures

J. Serre, A. Ghazali, and A. Gold*

*Groupe de Physique des Solides de l'Ecole Normale Supérieure, Université de Paris VII, Tour 23, 2 place Jussieu,
F-75251 Paris CEDEX 05, France*

(Received 16 March 1988)

We have investigated in quantum wells (QW's) and heterostructures (HS's) the modification of the electronic structure near the band edge, which is induced by selective doping. The density of states has been calculated as a function of the relevant parameters, namely, carrier and impurity concentrations (and depletion concentrations for HS's), QW width, and impurity position. Using a multiple-scattering method which includes a finite-range screened potential and impurity concentration to all orders, we have succeeded in obtaining ground-state and excited-state impurity bands (IB's). We observed these bands merging gradually with the lowest conduction subband as the impurity concentration is increased, leading to the formation of a band tail into the energy gap. Other main results obtained for different values of the parameters are the binding energy for a single impurity, the widths and energy shifts of ground- and excited-state IB's, and the contribution of the electron-impurity interaction to the gap shrinkage in the band-tail regime. Our results are compared with experiments and other theories.

I. INTRODUCTION

It is well known that charged impurities play a fundamental role in determining the electronic, optical, and transport properties of quantum wells (QW's) and heterostructures (HS's). The effects of impurities have been widely studied during the last years both theoretically and experimentally.

Most of the theoretical work on $\text{Al}_x\text{Ga}_{1-x}\text{As}/\text{GaAs}/\text{Al}_x\text{Ga}_{1-x}\text{As}$ QW's considered a single hydrogenic impurity, using variational wave functions to obtain ground- and excited-state levels. In an early work, Bastard¹ calculated the binding energy as a function of QW width and of impurity position, assuming an infinite barrier height. Since then, a large number of works have attempted to improve this model. Mailhot *et al.*,² Greene and Bajaj,³ and Liu and Quinn⁴ considered the case of finite barrier height. Brum *et al.*⁵ showed how the binding energy of a single impurity is reduced by the free-carrier screening. Excited states have also been studied extensively.^{2,3,6-8} The influence of a magnetic field applied along the growth axis has also deserved particular attention.^{9,10} Good reviews of theoretical works on the electronic structure of impurities and experimental work on extrinsic optical properties in QW's have recently been offered by McCombe *et al.*¹¹ and by Shanabrook.¹¹ For low impurity concentrations, the theoretical results generally agree with the experimental ones obtained by far-infrared (magneto-) absorption, electronic Raman scattering, photoluminescence, etc. For a more detailed discussion and references, see Ref. 11.

Theoretically, the influence of charged impurities on the mobility has been widely studied in $\text{Al}_x\text{Ga}_{1-x}\text{As}/\text{GaAs}$ HS's (Refs. 12-14) and QW's,¹⁵⁻¹⁷ following the work of Stern and Howard.¹⁸ All these cal-

culations are made within the Born approximation. One of us has studied static and dynamic transport properties in HS's (Ref. 19) and QW's (Ref. 20) accounting for multiple-scattering effects.

The aim of this paper is to study the situation where the impurity concentration is high enough for the single-impurity theory to be no longer valid, i.e., when the overlap of impurity wave functions becomes significant. We use a multiple-scattering theory method which accounts for the electron-impurity interaction to all orders in the impurity concentration and to all orders in the electron-impurity potential. Many-body effects, namely screening and exchange-correlation contributions to the self-energy, are also included in our calculations.

In this paper we calculate the density of states (DOS) of impurity bands (IB's) in the ground state as well as in excited states and the DOS of the first conduction subband (CSB) edge. These calculations are made for different values of the relevant parameters, namely the impurity and electron concentrations and the position of impurities, the width of the QW, and the depletion concentration of the HS. In particular, we are able to show the broadening and the gradual merging of excited and ground IB states with the CSB, as the impurity concentration is increased to make up a band tail (BT).

Different attempts have been made in order to estimate the effects of charged impurities on the DOS in the vicinity of the bottom of the CSB. Because the binding energy is strongly dependent on the position of the impurities in and near the well, an IB has been predicted for a homogeneous doping of the well,^{1,21} even if the concentration is low enough to neglect an impurity wave-function overlap. However, this description is not strictly valid when the overlap occurs, because the global DOS is not merely the sum of individual contributions arising from impuri-

ties located at different positions. This point will be discussed later.

Takeshima²² studied the deformation of the CSB in the presence of charged impurities. However, his assumption of a slowly varying potential which might be valid only for heavy doping does not allow us to obtain an IB. De Andrada e Silva and da Cunha Lima²³ calculated the DOS of an IB in $\text{Al}_x\text{Ga}_{1-x}\text{As}/\text{GaAs}$ QW's, using a tight-binding version of the multiple-scattering theory. It is essentially a single-band scheme. Indeed, the IB is not treated as a result of a perturbation of the CSB but rather as a single band in an amorphouslike solid. This is the reason why this CSB cannot be accounted for in their model. In particular, an IB should persist even at a very high impurity density.

The multiple-scattering method used here was employed by the present authors^{24,25} to study the IB's and BT's in inversion and accumulation layers in silicon metal-oxide-semiconductor (MOS) structures. Our results are in semiquantitative agreement with a recent experimental study²⁶ where the IB's and BT's are probed by varying the carrier concentration. As said before, our method, based on the best Klauder's²⁷ multiple-scattering approach, uses an infinite perturbation series expansion in powers of the potential strength and concentration.²⁸ Although this method does not account for the so-called multiple-occupancy corrections, we believe that these corrections are negligible for the usual impurity concentrations, see the discussion in Ref. 28, Appendix B. In particular, starting from the unperturbed CSB wave function, ground and excited IB's are obtained for low impurity concentrations.

The paper is organized as follows. In Sec. II the theory and the model for QW's and HS's are explained. The results for QW's and HS's are given in Secs. III and IV, respectively. They are discussed and compared with other theoretical and experimental results in Sec. V. A summary is given in Sec. VI.

II. THEORY AND MODEL

A. Density of states

In this section we briefly recall the multiple-scattering equations leading to the electronic density of states (DOS). A detailed account of the theory has been given by Serre and Ghazali in the three-dimensional case.²⁸ This theory has been applied by the present authors to inversion and accumulation layers.^{24,25}

In order to describe the one-electron properties of the interacting electron system in the presence of impurities, we use the average one-electron Green function $G(\mathbf{k}, E)$ for wave vector \mathbf{k} and energy E

$$G(\mathbf{k}, E) = \frac{1}{E - \varepsilon(\mathbf{k}) - \Sigma(\mathbf{k}, E)} \quad (1)$$

$\varepsilon(\mathbf{k})$ is the kinetic energy of the electron in the unperturbed system. A parabolic dispersion relation in a single conduction subband with an effective mass m^* is used: $\varepsilon(\mathbf{k}) = \hbar^2 k^2 / 2m^*$.

The self-energy $\Sigma(\mathbf{k}, E)$ has two contributions: the

exchange-correlation self-energy $\Sigma_{xc}(\mathbf{k}, E)$ which is due to electron-electron interactions, and the electron-impurity self-energy $\Sigma_{ei}(\mathbf{k}, E)$ which is due to the scattering by impurities randomly distributed in the system

$$\Sigma(\mathbf{k}, E) = \Sigma_{xc}(\mathbf{k}, E) + \Sigma_{ei}(\mathbf{k}, E) \quad (2)$$

The average probability of the electron with energy E being in the state \mathbf{k} is given by the spectral density $A(\mathbf{k}, E)$ via

$$A(\mathbf{k}, E) = -\frac{1}{\pi} \text{Im} G(\mathbf{k}, E + i0) \quad (3)$$

and the DOS per unit energy and per unit volume, $\rho(E)$, is given by

$$\rho(E) = \frac{1}{\Omega} \sum_{\mathbf{k}, \sigma} A(\mathbf{k}, E) \quad (4)$$

The summation is over the \mathbf{k} 's and the spin states σ . Ω is the area.

We calculate the self-energy for electron-impurity interaction $\Sigma_{ei}(\mathbf{k}, E)$ in Klauder's best (fifth) multiple-scattering approximation.²⁷ $\Sigma_{ei}(\mathbf{k}, E)$ is given²⁴ in terms of the two-dimensional (2D) impurity concentration N_I , the 2D Fourier transform of the electron-impurity interaction potential $V(\mathbf{q})$, and the vertex function $U(\mathbf{k}, \mathbf{q}, E)$ which obeys an integral equation, see Eq. (6) in Ref. 24. This integral equation for U is nonlinear.²⁸

The separable-potential approximation (SPA) for the electron-impurity interaction

$$V(\mathbf{q} - \mathbf{q}') = \frac{\pi}{2} [V(q)]^{1/2} [V(q')]^{1/2} \quad (5)$$

allows the transformation of the integral equation (6) (Ref. 24) into a much simpler equation. This equation (5) is exactly valid for a contact potential, but it is only an approximation for a finite-range potential. However, results obtained for the three-dimensional²⁹ and two-dimensional^{24,25} system have proved reasonable when compared with exact results. Furthermore, the binding energy can be calculated analytically in the limit $N_I \rightarrow 0$.²⁴

Within the SPA the binding energy E_B is determined by

$$\frac{1}{\pi^2} \int_0^\infty dq q V(q) \frac{1}{E_B + q^2 / 2m^*} = 1 \quad (6)$$

We use the SPA in the limit $N_I \rightarrow 0$ where the convergence in the full Klauder's fifth approximation is hardly obtainable for computer time reasons. It is also used when systematic studies are needed.

B. Quantum-well and heterostructure models

Let us first describe the QW model. In the unperturbed medium, the electrons can move freely in the x - y plane and are confined in the z direction. We consider the case involving only the lowest conduction subband. In the infinite barrier height approximation, the wave function $\psi(z)$ for the z direction and for the lowest subband is given by

$$\psi(z) = \left[\frac{2}{L} \right]^{1/2} \sin \left[\frac{\pi z}{L} \right], \quad 0 \leq z \leq L \quad (7)$$

and is zero elsewhere. Here L is the QW width: see Fig. 1(a). We assume that donors with a 2D concentration N_i are implanted randomly in a plane parallel to the x - y plane at a distance z_i from the QW edge ($z=0$), see Fig. 1(a).

We consider a screened electron-impurity interaction

$$V(\mathbf{q}) = \frac{V_{ei}(\mathbf{q})}{\epsilon(\mathbf{q})}, \quad (8)$$

where $\epsilon(\mathbf{q})$ is the dielectric function of the interacting electron gas.

The unscreened electron-impurity potential $V_{ei}(q)$ for wave number q is given by

$$V_{ei}(q) = \frac{2\pi e^2}{\epsilon_L} \frac{1}{q} F_{ei}(q, z_i), \quad (9)$$

where ϵ_L is the dielectric constant of the host lattice. It is equal to the half sum of dielectric constants in the QW and in the surrounding medium. The electron-impurity form factor F_{ei} accounts for the finite extension of the wave function in the z direction, see Ref. 30, Sec. IV.C.1. One finds for QW's (Ref. 20)

$$F_{ei}(q, z_i) = \frac{8\pi^2}{qL} \frac{1}{4\pi^2 + q^2 L^2} + \begin{cases} [1 - \exp(-qL)] \exp(qz_i)/2, & z_i < 0 \\ [1 - \exp(-qz_i)]/2 - \exp[-q(l - z_i)]/2 + q^2 L^2 \sin^2(\pi z_i/L)/2\pi^2, & 0 \leq z_i \leq L \\ [1 - \exp(-qL)] \exp[-q(z_i - L)]/2, & z_i > L \end{cases} \quad (10a)$$

$$[1 - \exp(-qz_i)]/2 - \exp[-q(l - z_i)]/2 + q^2 L^2 \sin^2(\pi z_i/L)/2\pi^2, \quad 0 \leq z_i \leq L \quad (10b)$$

$$[1 - \exp(-qL)] \exp[-q(z_i - L)]/2, \quad z_i > L \quad (10c)$$

For the dielectric function we use the random-phase approximation (RPA) (Ref. 31) with local field (exchange-correlation) correction;³² see Eq. (13) in Ref. 24. $V_C(q)$ is the electron-electron interaction potential, which enters the dielectric function and which includes the 2D Coulomb potential and the form factor which accounts for the finite confinement (see Ref. 30, Sec. II.F.1). It is given by

$$V_C(q) = \frac{2\pi e^2}{\epsilon_L} \frac{1}{q} F_C(q). \quad (11)$$

For QW's one gets²⁰

$$F_C(q) = \frac{1}{4\pi^2 + q^2 L^2} \times \left[3aq + \frac{8\pi^2}{qL} - \frac{32\pi^4}{q^2 L^2} \frac{1 - \exp(-qL)}{4\pi^2 + q^2 L^2} \right]. \quad (12)$$

Equations (8)–(12) specify $V(\mathbf{q})$ which enters Eqs. (1)–(4) for the calculation of the self-energy $\Sigma_{ei}(\mathbf{k}, E)$. For the exchange-correlation self-energy Σ_{xc} we take, as in

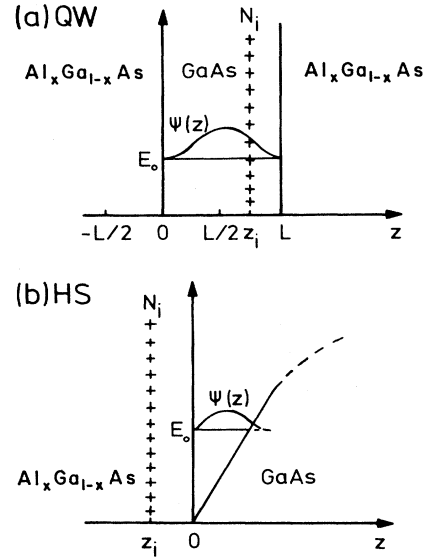


FIG. 1. Sketch of (a) $\text{Al}_x\text{Ga}_{1-x}\text{As}/\text{GaAs}/\text{Al}_x\text{Ga}_{1-x}\text{As}$ quantum well (QW) and (b) $\text{Al}_x\text{Ga}_{1-x}\text{As}/\text{GaAs}$ heterostructures (HS). In both cases the origin of the growth axis z is taken at the (left) interface.

Ref. 24, and E - and k -independent self-energy which is obtained as a fit of numerical results of Vinter³³ for silicon MOS structures, see Eq. (18) in Ref. 24.

Let us now turn to the HS model; see Fig. 1(b). As for QW's we only consider the lowest conduction subband and assume an infinite barrier height. In this case, the variational form of the wave function in the z direction is taken as [see Ref. 30, Eq. (3.25)]

$$\psi(z) = (b^3/2)^{1/2} z \exp(-bz/2). \quad (13)$$

The quantity $1/b$ measures the extension of the wave function in the bulk. In the triangular-well approximation, b is given by [see Ref. 30, Eq. (3.30)]

$$b^3 = \frac{48\pi e^2 m_z}{\epsilon_{\text{hs}} \hbar^2} (N_d + 11N/32), \quad (14)$$

where m_z is the effective mass perpendicular to the interface, ϵ_{hs} is the dielectric constant in the heterostructure, and N_d is the 2D depletion density.

The form factor E_{ei} in heterostructures is given by (see Ref. 30, Sec. II.C)

$$F_{ei}(q, z_i > 0) = \begin{cases} \frac{1}{(1-q/b)^3} [\exp(-qz_i) - (a_1 + a_2bz_i + a_3b^2z_i^2)\exp(-bz_i)], & q \neq b \\ [(1 + 2bz_i + 2b^2z_i^2 + 4b^3z_i^3/3)\exp(-bz_i)]/8, & q = b, \end{cases} \quad (15a)$$

and

$$F_{ei}(q, z_i \leq 0) = \exp(qz_i)/(1+q/b)^3 \quad (15b)$$

with $a_0 = 1 + q/b$, $a_1 = 2q(3 + q^2/b^2)/ba_0^3$, $a_2 = 4q(1 - q/b)/ba_0^2$, and $a_3 = q(1 - q/b)^2/ba_0$. The expression given in Eq. (24) is valid only if the dielectric constants on both sides of the HS are equal. This is the case which we have studied here. $F_{ei}(q, z_i > 0)$ is shown in Fig. 2 for various values of z_i . With increasing z_i , F_{ei} first increases and then decreases. The maximum is reached when the average distance of the envelope wave function from the interface $\langle z \rangle = 3/b$ is equal to z_i ; at this point the electron-impurity interaction is strongest.

The screening form factor $F_C(q)$, which enters the dielectric function [see Eq. (11)], is given by

$$F_C(q) = \frac{1 + 9q/8b + 3q^2/8b^2}{(1 + q/b)^3}. \quad (16)$$

Finally, let us emphasize that all the above presented equations are valid within the mentioned approximations regardless of the materials which constitute the QW's or the HS's.

C. GaAs-Al_xGa_{1-x}As structures

We have solved the equations for Al_xGa_{1-x}As/GaAs/Al_xGa_{1-x}As QW's and HS's. The dielectric constants and effective masses are assumed to be equal in both materials. The DOS will be given with a spin degeneracy equal to 2 even for impurity bands, although a value of 1 is more reasonable in this case. The use of a

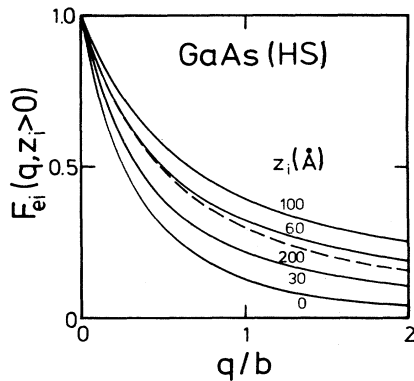


FIG. 2. Electron-impurity potential form factor F_{ei} for Al_xGa_{1-x}As/GaAs HS as a function of normalized wave number q/b for various values of the impurity position z_i , see Eq. (15). We used $b = 2/a^*$, see Eq. (14).

spin-independent potential model (as in our case) does not allow us to determine this degeneracy. The unit length is the effective Bohr radius $a^* = \epsilon_L \hbar^2 / m^* e^2 = 103 \text{ \AA}$, if we take $m^* = m_z = 0.067m_0$ and $\epsilon_L = 13.1$. The effective Rydberg is $R = m^* e^4 / 2\epsilon_L^2 \hbar^2 = 5.3 \text{ meV}$. The DOS is presented in units of $1/2\pi R a^*$; it is equal to 1 for free electrons in the lowest conduction subband. In real units, the DOS for free electrons is equal to $2.83 \times 10^{10} \text{ meV}^{-1} \text{ cm}^{-2}$. The origin of the energy scale is taken at the lowest subband edge, including exchange-correlation and band-bending energy shifts.

The electron concentrations and the QW widths used here are such that only the lowest conduction subband is involved. Our calculations are made within the infinite-barrier-height approximation.

Finally, let us mention that since our results are expressed in units of effective Rydberg R and effective Bohr radius a^* , they are valid for any hydrogenic impurity type and for 2D materials with a parabolic conduction (valence) subband.

III. RESULTS FOR QUANTUM WELLS

We have calculated the DOS of QW's for different values of the relevant parameters, namely the well width L , the position of impurities z_i (inside and outside the well), the 2D impurity concentration N_i , and the carrier concentration N in the well. For a given set of these parameters, the spectral density $A(\mathbf{k}, E)$ as a function of \mathbf{k} [Eq. (3)] and the DOS [Eq. (4)] are calculated for different energies near the bottom of the lowest conduction subband.

A. Impurity band and band tail

Figure 3 shows the broadening and the shift of the single hydrogenic impurity level as the impurity concentration N_i increases. This leads to an IB split off from the lowest CSB. As N_i is further increased, these bands get closer, fill up the gap in between at a certain concentration \tilde{N}_i , and finally merge to give a BT. Figure 3 is obtained for a QW with $L = 100 \text{ \AA}$. Here, the impurities are in the middle of the well and $N = N_i$.

The spectral density $A(\mathbf{k}, E)$ is displayed in the inset of Fig. 3 for $N = N_i = 2 \times 10^{10} \text{ cm}^{-2}$ and for two energies, one in the main band and the other in the impurity band. The spectral density which is a δ function centered at $\mathbf{k} \neq 0$ for a free electron is now broadened in \mathbf{k} space for the states lying at the bottom of the subband because of impurity scattering. In the IB, $A(\mathbf{k}, E)$ is maximum at $\mathbf{k} = 0$ and widely extended in \mathbf{k} space. This behavior is typical for localized quasiatomic electrons.²⁸

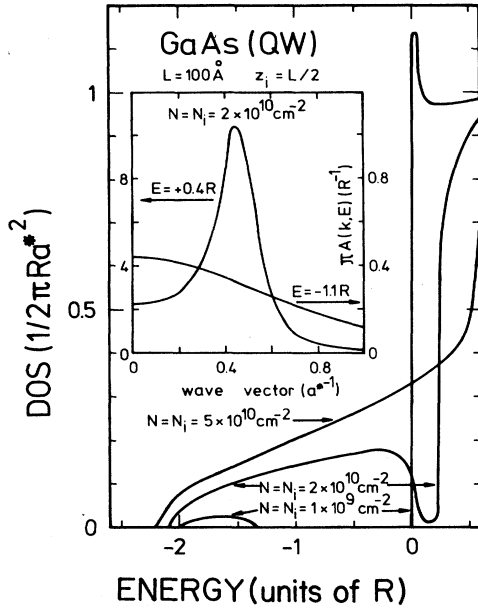


FIG. 3. Density of states (DOS) as a function of energy for different values of electron density N and impurity density N_i . The electron-impurity potential is screened according to the exchange-correlation-corrected random-phase approximation (RPA), see Sec. II A. The impurities are located at the center of the QW of width L . The inset shows the typical spectral densities as functions of wave number for a quasiextended state ($E = 0.4R$) and for a quasiautomic state ($E = -1.1R$).

B. Role of screening

For given L , z_i , and N_i the locations of the IB edges vary with carrier concentration because of screening. The impurity bandwidth decreases as N increases. The curves in Fig. 4 illustrate this behavior. They are obtained for a rather low N_i in order to compare our results with those of Brum *et al.*⁵ which have been obtained for the same geometry, but in the single-impurity limit. Like these authors, we obtain a small gap for high N , which is nearly constant, see Fig. 4. However, it is clear that for higher N_i a merging of the bands is expected, see Fig. 3.

The curves in Fig. 5 show the effect of screening on the location of the IB edges within the SPA for different N_i . Three remarks are in order. (i) The SPA results agree semiquantitatively with the full calculation results; compare Figs. 4 and 5. (ii) However, the IB in the latter case lies always at energies below those obtained in the SPA. (iii) It is worthwhile to notice that the width of the IB increases drastically with increasing N_i . For example, with $N = 1 \times 10^{10} \text{ cm}^{-2}$ the width increases from $0.45R$ for $N_i = 1 \times 10^9 \text{ cm}^{-2}$ to $1.35R$ for $N_i = 1 \times 10^{10} \text{ cm}^{-2}$; see Fig. 5.

C. Influence of the QW width and impurity position

The IB edge energies strongly depend on the position of impurities relative to the well. As illustrated in Fig. 6,

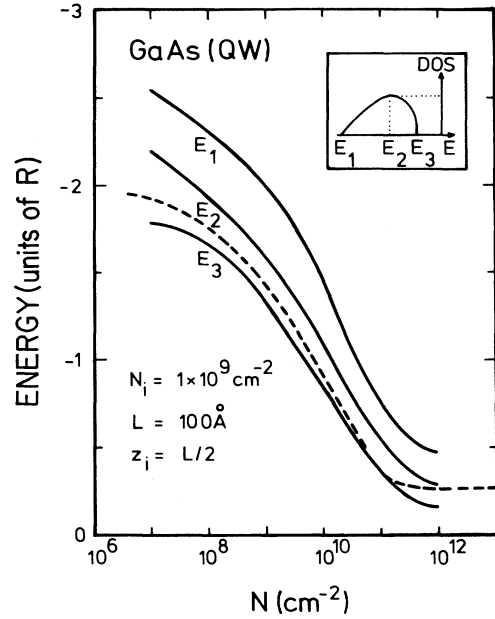


FIG. 4. Solid lines: Impurity-band energies (see inset) as functions of electron density N for given N_i , z_i , and L . Dashed line: Binding energy of a single impurity for the same L and z_i , taken from Brum *et al.* (Ref. 5).

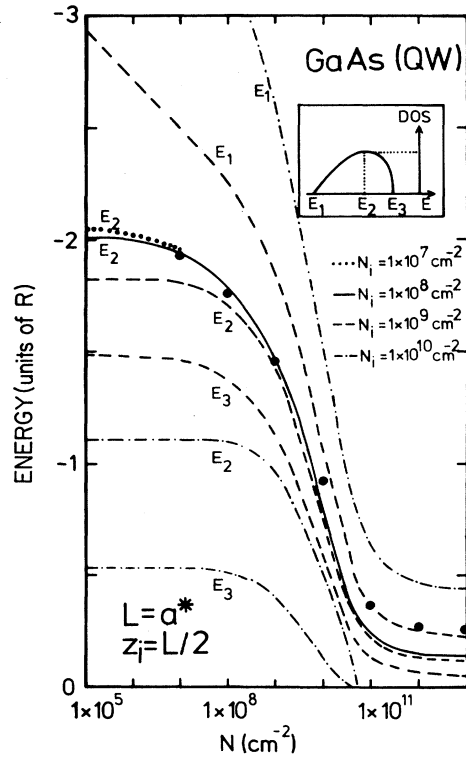


FIG. 5. Impurity-band energies (see inset) as functions of electron density N for different N_i , calculated in the separable-potential approximation for the same geometry as in Fig. 4. The solid points represent Brum *et al.* results (Ref. 5).

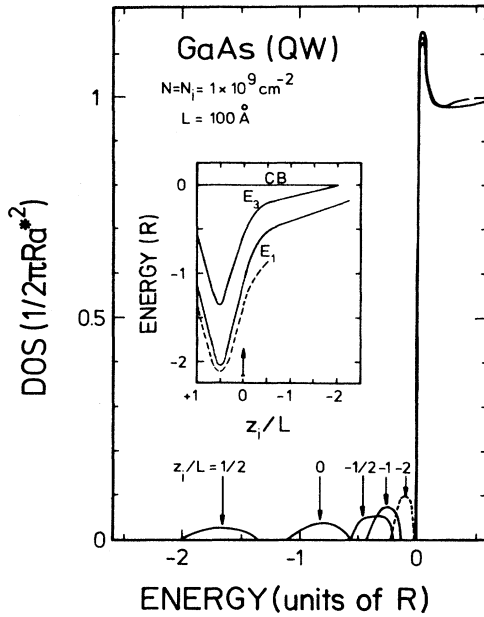


FIG. 6. Effect of impurity position z_i on the shift and broadening of the impurity band (IB). The inset shows the IB and the conduction subband (CSB) edge energies as functions of z_i (solid lines). The dashed line represents the calculation of Lane and Greene (Ref. 8) for the single-impurity limit.

starting from an IB centered at $-1.7R$ with impurities being in the middle of the QW, the IB moves towards the CSB as the impurities are distanced further and further from the well. In this example, the IB is pushed against the CSB when the impurities are placed at 200 \AA from the QW barrier. In order to compare our results with those obtained in the single-impurity limit, we have shown recent results calculated by Lane and Greene⁸ in the inset of Fig. 6. Figure 6 illustrates that the IB is less symmetric when it is closer to the CSB. At the same time, the width of the IB shrinks (and the DOS maximum increases). The asymmetry of the IB has also been obtained in the three-dimensional case²⁸ and in the two-dimensional case for silicon MOS systems.^{24,25}

For a systematic study of the influence of L and z_i on the band structure we have used the SPA. Figure 7 shows the band edges as functions of N_i for $L = 100$ and 300 \AA and for $z_i = L/2$ [Fig. 7(a)], $z_i = 0$ [Fig. 7(b)], and $z_i = -L$ [Fig. 7(c)]. We have taken $N = N_i$. The band-edge energies E_1 and E_3 are defined in the inset of Fig. 4. For reasons of comparison, band-edge energies obtained by the full calculations are also indicated for $N = N_i = 1 \times 10^9 \text{ cm}^{-2}$ in these figures. One notes that the IB meets the CSB at $\tilde{N}_i = 2 \times 10^{10} \text{ cm}^{-2}$ for impurities located at the center of the QW. For N_i larger than \tilde{N}_i , a band tail appears and broadens as N_i increases. As seen in the figure, \tilde{N}_i goes down to $2.5 \times 10^9 \text{ cm}^{-2}$ for impurities located at 100 \AA from the QW edge. The values of \tilde{N}_i for the same z_i 's are lower for a wider well, see Fig. 7, because the mean distance between electrons and impurities is larger as the QW is wider.

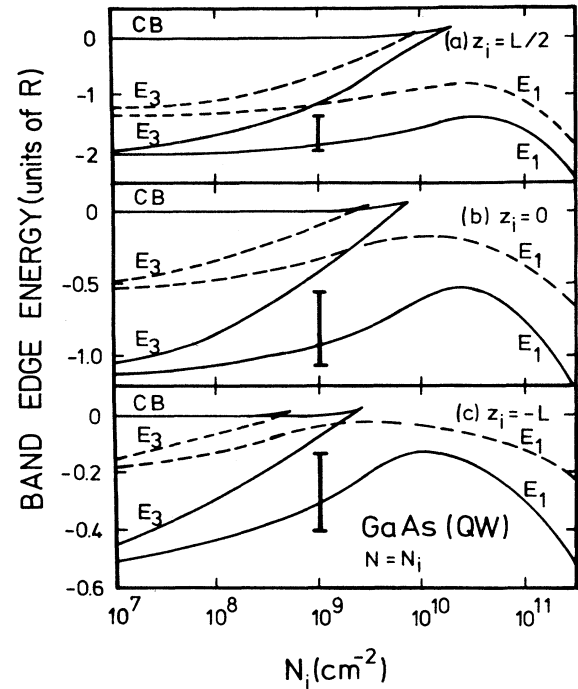


FIG. 7. IB and CSB edge energies as functions of impurity concentration (here $N = N_i$) for $L = 100 \text{ \AA}$ (solid lines) and $L = 300 \text{ \AA}$ (dashed lines). Impurities are located: (a) at the QW center, (b) at the QW edge, and (c) in the barrier (at a distance from the QW edge equal to the QW width). The calculations are made in the separable-potential approximation. The vertical bars indicate the IB location as obtained by the full calculations for $L = 100 \text{ \AA}$.

As mentioned in Sec. II A, the SPA is used in the limit $N_i \rightarrow 0$ to calculate the binding energy E_B . E_B is obtained from Eq. (6). Figure 8 illustrates the decrease of E_B for different values of z_i as the QW width increases. These results are in good agreement with the results of Bastard.¹ One also notices the rapid decrease in the binding energy as a function of L in case of narrow QW's with remote impurities ($z_i < 0$). For comparison purposes, some IB edge energies obtained by the full calculations are also indicated in Fig. 8 for small concentrations: $N = 1 \times 10^7 \text{ cm}^{-2}$ and $N_i = 1 \times 10^8 \text{ cm}^{-2}$. Note, however, that these concentrations are lower than the residual concentrations usually found in these materials.

A systematic study of \tilde{N}_i (the impurity density for which IB and CSB meet) and E_B as a function of impurity position is shown in Fig. 9 for $L = 100$ and 300 \AA within the SPA. An unscreened electron-impurity interaction [Fig. 9(a)] and the RPA screening model [Figs. 9(b) and 9(c)] have been used. \tilde{N}_i is obtained after calculating the DOS's as functions of the energy for different N_i and after searching for the IB-CSB zero-gap band-limit. It is worth noticing that \tilde{N}_i and E_B vary in the same way as functions of z_i . Similar results have been found in silicon inversion layers.²⁵ This is not surprising

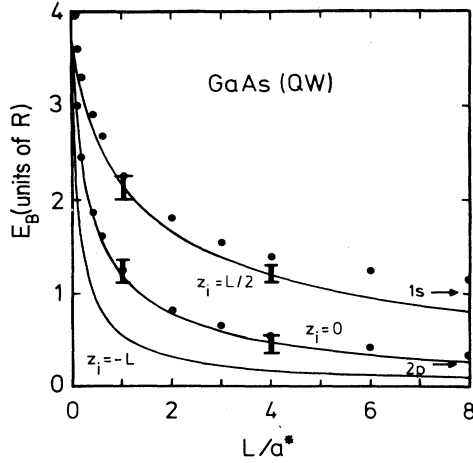


FIG. 8. Binding energy of a single impurity as a function of the QW width for different z_i . Solid lines: Separable-potential approximation. The dots represent the results of Bastard (Ref. 1). The bars indicate the IB locations for low concentration: $N_i = 1 \times 10^8 \text{ cm}^{-2}$, $N = 1 \times 10^7 \text{ cm}^{-2}$.

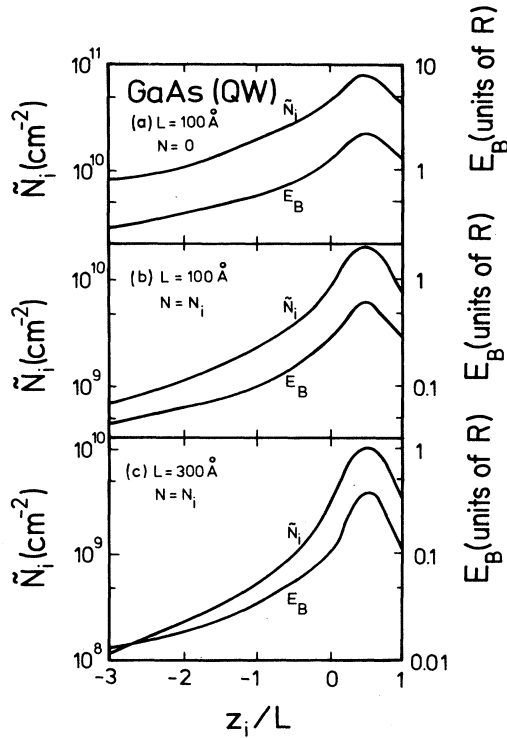


FIG. 9. Impurity concentration \tilde{N}_i at the closing of the gap between IB and CSB (left) and binding energy E_B (right) as functions of impurity position z_i within the separable-potential approximation: (a) $L = 100 \text{ \AA}$, $N = 0$ (no screening), (b) $L = 100 \text{ \AA}$, and (c) $L = 300 \text{ \AA}$. For (b) and (c) we used $N = \tilde{N}_i$ for all \tilde{N}_i 's (screening), E_B is calculated for $N = \tilde{N}_i$ and $N_i \rightarrow 0$. Note the strong decrease in \tilde{N}_i and E_B in the screened case.

since both \tilde{N}_i and E_B measure the potential strength. We find that the ratio \tilde{N}_i/E_B is nearly constant and given by

$$\tilde{N}_i/E_B \approx [(1-4) \times 10^{10} \text{ cm}^{-2}] R^{-1}. \quad (17)$$

The CSB energy shift E_{ei} due to electron-impurity interactions is found to obey approximately the following law:

$$E_{ei} = -\alpha [N_i / (10^{11} \text{ cm}^{-2})]^\beta. \quad (18)$$

In Fig. 10 α and β are displayed versus z_i for $L = 100$ and 300 \AA . We notice that β is independent of z_i and nearly equal to 0.5. In principle, our disorder-induced band-gap renormalization must be added to the other sources of the CSB shift: (i) the negative exchange-correlation shift, see recent experiments on QW's,³⁴ and (ii) the positive Coulomb shift due to electrostatic interactions, see, e.g., Ref. 5.

D. Excited impurity bands

We have studied the possible existence of excited IB's in a QW, using the full calculations. As we will see below, such bands do exist in a certain range of concentrations N and N_i . It should be mentioned, however, that within the SPA no such bands were obtained.

As an example, we show in Fig. 11 results for a QW with $L = 100 \text{ \AA}$. Impurities with a concentration $N_i = 1 \times 10^9 \text{ cm}^{-2}$ are located in the middle of the well. Three electron concentrations are considered: $N = 1 \times 10^7$, 1×10^8 , and $1 \times 10^9 \text{ cm}^{-2}$. For reasons of completeness, we show in Fig. 11 the IB DOS's in the ground state (1s state), whose integrated DOS is equal to N_i . The band-edge energies of these 1s IB's have been shown in Fig. 4, where the influence of screening was illustrated. The role of screening is even more essential to the very

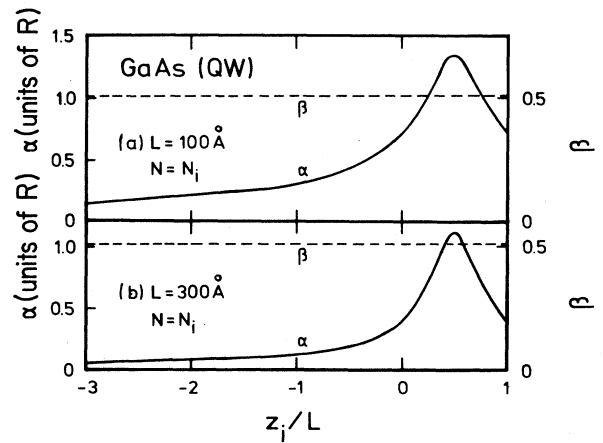


FIG. 10. Prefactor α (left) and exponent β (right), see Eq. (18), which gives the electron-impurity contribution to the gap shrinkage, as a function of impurity position z_i . The calculations are made within the separable-potential approximation: (a) $L = 100 \text{ \AA}$ and (b) $L = 300 \text{ \AA}$. In both cases we used $N = N_i$.

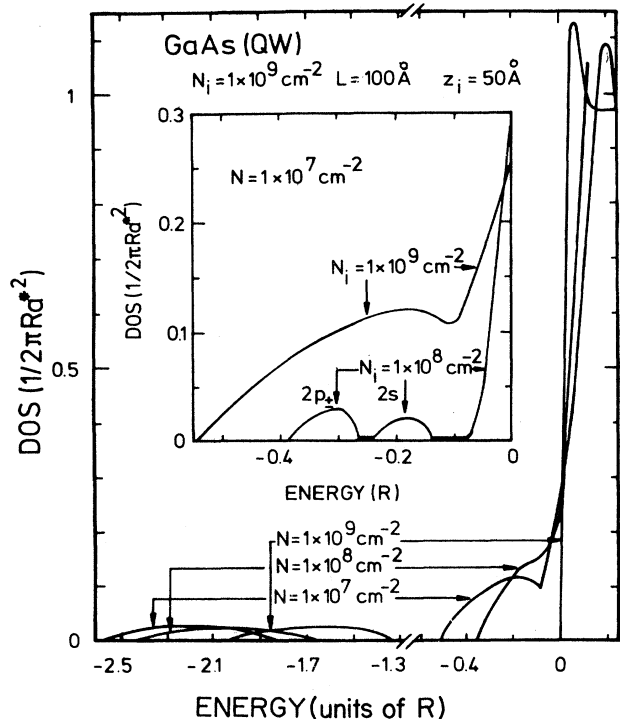


FIG. 11. DOS as a function of energy of ground- and excited-state IB's and of the CSB edge for $N_i = 1 \times 10^9 \text{ cm}^{-2}$ and for different carrier concentrations. The inset shows the splitting of the excited IB state into $2p_{\pm}$ and $2s$ for $N = 1 \times 10^7 \text{ cm}^{-2}$ as N_i is decreased.

existence of excited IB's, as shown in Fig. 11. For higher electron concentration ($N = 1 \times 10^9 \text{ cm}^{-2}$), no excited IB is obtained. For $N = 1 \times 10^8 \text{ cm}^{-2}$ a band tail appears and changes into an almost-split-off excited IB at $N = 1 \times 10^7 \text{ cm}^{-2}$. The integrated DOS of this IB is approximately equal to $3N_i$. In order to identify the nature of this excited IB, we have taken a lower impurity concentration ($N_i = 1 \times 10^8 \text{ cm}^{-2}$). As can be seen in the inset of Fig. 11, the excited IB DOS is now broken up into two separate IB's. The lower- and the higher-energy IB's have integrated DOS's equal to $2N_i$ and N_i , respectively. We have thus identified the former IB to be the doubly degenerate $2p_{\pm}$ IB and the latter to be the nondegenerate $2s$ IB.³ These results are confirmed in other situations, see Figs. 12 and 13. Another confirmation of the fact that these excited bands have different symmetries is given by the quite different spectral density shapes for the $2p_{\pm}$ and $2s$ IB's, see the insets of Figs. 12 and 13.

For much larger QW width ($L = 800 \text{ \AA}$), see Fig. 13, in addition to $2p_{\pm}$ and $2s$ IB's, a shoulder appears in the DOS at the bottom of the CSB, which we attribute to the onset of the $2p_0$ IB. This band is reminiscent of the $2p_z$ IB in the three-dimensional system. In contrast to this situation, for a rather narrow QW ($L = 100 \text{ \AA}$) and for the same concentrations as above, the $2p_0$ IB is no longer seen, as illustrated in Fig. 12. This confirms the more

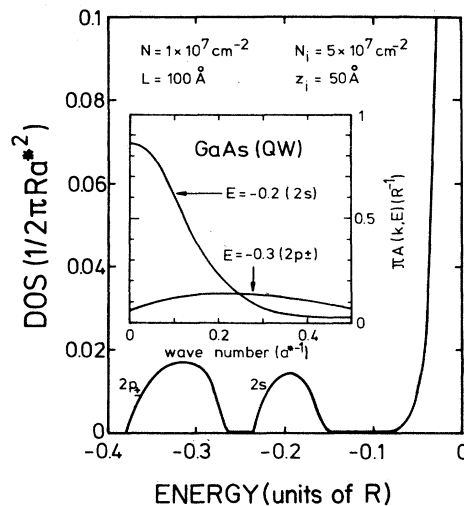


FIG. 12. DOS vs energy of the $2p_{\pm}$ and $2s$ IB's and of the CSB edge for low electron and impurity concentrations. In the inset the typical $2p_{\pm}$ and $2s$ spectral densities are plotted as functions of the wave number. We used $L = 100 \text{ \AA}$ and $z_i = 50 \text{ \AA}$.

pronounced 2D character in the latter case.

The relative energy positions of excited IB's $2p_{\pm}$, $2s$, and $2p_0$ as well as the appearance of the $2p_0$ IB for a wide-enough QW are in agreement with what was obtained for the single-impurity excited levels.^{2,3,6-8} As a last remark, let us mention that the gap between $1s$ and $2p_{\pm}$ is nearly independent of electron concentration, see Fig. 11. This suggests that the screening only has little influence on this gap.

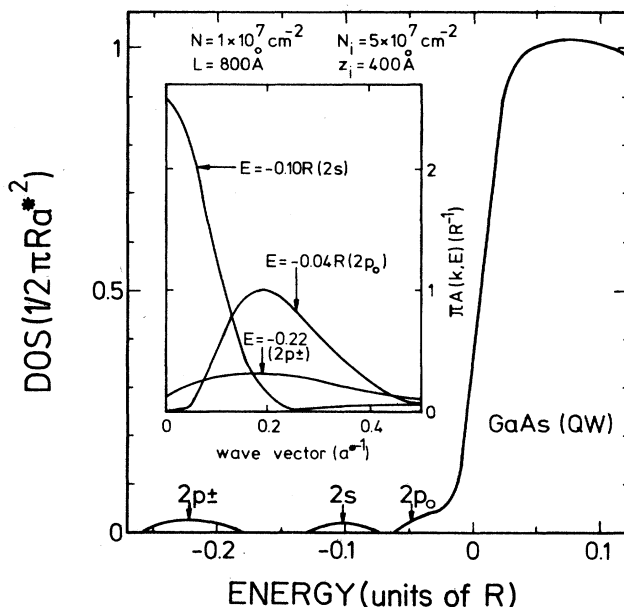


FIG. 13. DOS vs energy with $L = 800 \text{ \AA}$ and $z_i = 400 \text{ \AA}$, compare with Fig. 12. Note the appearance of the $2p_0$ IB.

IV. RESULTS FOR HETEROSTRUCTURES

We have calculated the DOS for heterostructures. The relevant parameters have been defined in Sec. II B. The 2D carrier concentration N and the 2D depletion layer concentration N_d determine the quantity $1/b$, see Eq. (14), which measures the extension of the wave function into the bulk. We have studied the case where the impurities are located in the $\text{Al}_{1-x}\text{Ga}_x\text{As}$ side ($z_i < 0$) and the case where they are located on the GaAs side ($z_i > 0$), see Fig. 1(b).

A. Impurity band and band tail

Figure 14 illustrates the continuous change from an IB to a BT as the impurity concentration is increased for a HS, defined by N and N_d . The impurities are located in the GaAs with a distance $z_i = 3/b$ from the interface. This distance is the average penetration of the electron charge into the GaAs bulk material. As seen in Fig. 14, the concentration \tilde{N}_i for which the IB and the CSB meet is $5 \times 10^9 \text{ cm}^{-2}$. It is clear that \tilde{N}_i should be higher if the electron concentration is lower. Indeed, the screening effect dominates the opposite effect of HS well widening, see Eq. (23). This has also been obtained for silicon MOS.²⁴

The influence of the impurity position z_i on the DOS is illustrated in Fig. 15. Starting from a situation where an IB separated from the main band, when the impurities were placed in the HS well ($z_i = 3/b$), one finds nearly a zero band gap for impurities at the interface ($z_i = 0$), and finally a BT is found for impurities located outside the well ($z_i = -a^*$). Let us mention that the impurity potential is strongly screened in this case and that no excited-state IB's exist.

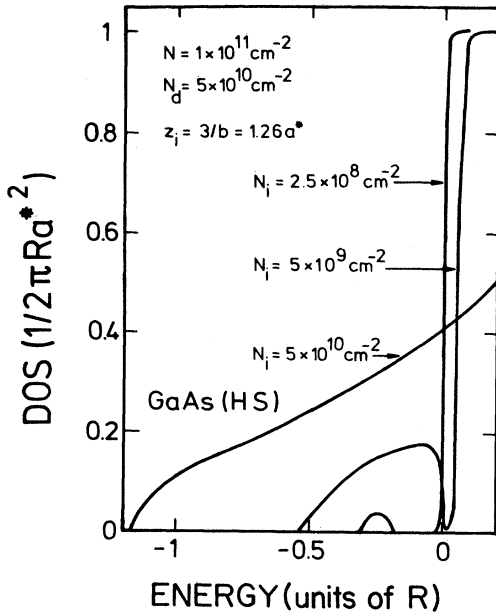


FIG. 14. DOS vs energy for heterostructures and for various values of N_i and given N , N_d , and z_i .

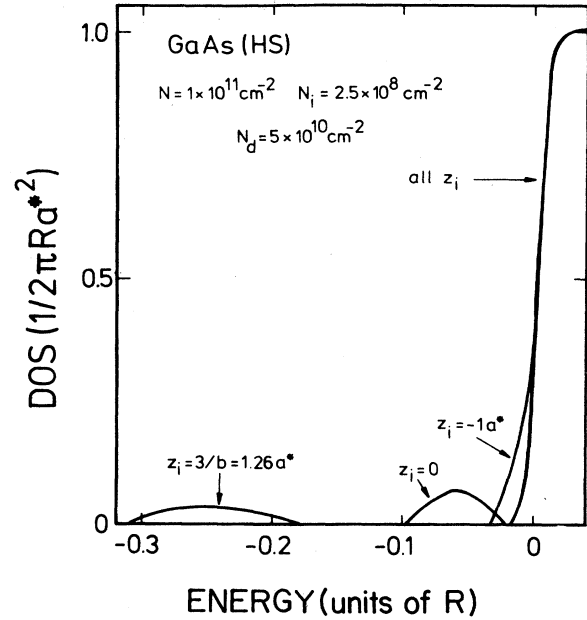


FIG. 15. Influence of the impurity position z_i on the width and on the energy shift of the IB in a HS. Notice the disappearance of the IB for $z_i < -a^*$ in this example.

B. Onset of IB gap closing and BT shift

Using the SPA, we have performed a systematic study of the DOS as a function of N , N_i , and z_i . The results are summarized in Fig. 16, where the variation of \tilde{N}_i and E_B as a function of z_i is displayed for an unscreened

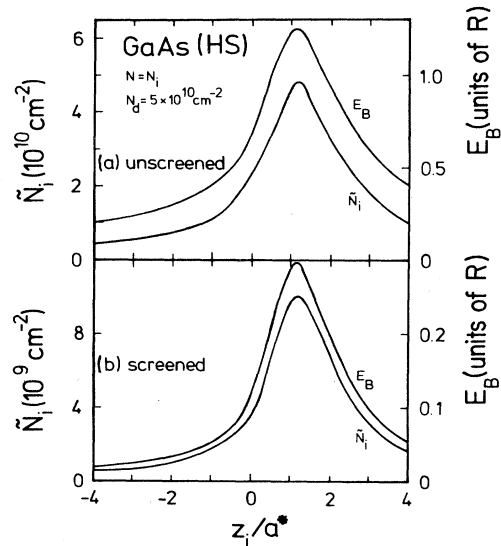


FIG. 16. Variation of \tilde{N}_i and E_B as functions of impurity position z_i within the separable potential approximation for (a) an unscreened potential (N is used here only to define the parameter b of the HS), and (b) a screened potential. We used $N = N_i$ and $N_d = 5 \times 10^{10} \text{ cm}^{-2}$. Note the strong decrease in \tilde{N}_i and E_B in the screened case.

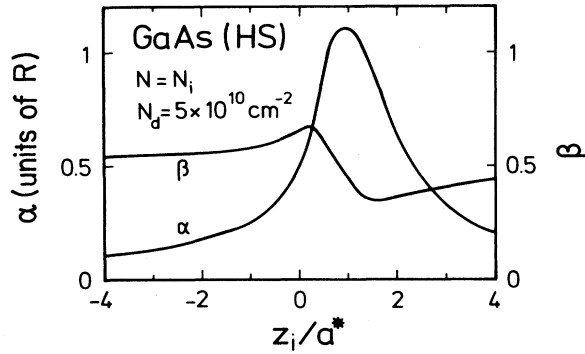


FIG. 17. Prefactor α (left) and exponent β (right) as functions of impurity position z_i , see Eq. (18) and Fig. 10. We used $N = N_i$ and $N_d = 5 \times 10^{10} \text{ cm}^{-2}$. The calculation was made in the separable-potential approximation.

electron-impurity interaction potential [Fig. 16(a)] and for a RPA-screened electron-impurity interaction potential, $N = N_i$ [Fig. 16(b)]. To our knowledge no single-impurity binding-energy calculations have been made so far on HS's as a function of z_i . As expected, \tilde{N}_i and E_B are much higher in the unscreened case and when the impurities are placed closer to the electrons in the HS well. Again we find that the ratio \tilde{N}_i/E_B is nearly constant, see Eq. (17) and our results for silicon MOS structures.²⁵

Like QW's (Sec. III C) and silicon MOS systems,²⁴ the BT shift towards low energies brought about by electron-impurity interactions obeys the law given by Eq. (18). Figure 17 shows α and β as functions of z_i for $n_d = 5 \times 10^{10} \text{ cm}^{-2}$ and for $N = N_i$. In this case β is not constant as found for QW's and varies weakly around 0.5

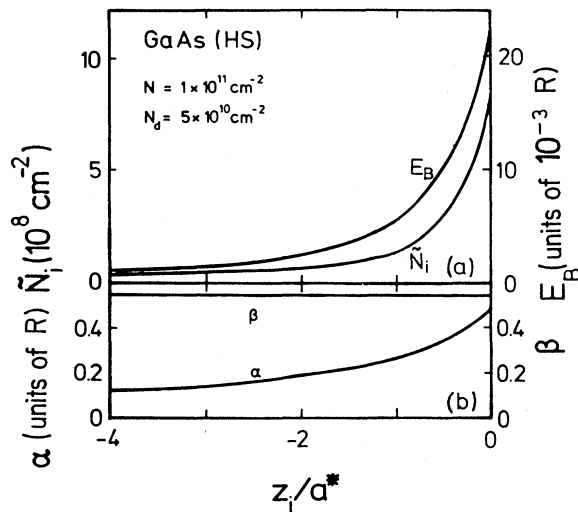


FIG. 18. Variation of (a) \tilde{N}_i and E_B and (b) α and β [Eq. (18)] as functions of z_i for a HS with $N = 1 \times 10^{11} \text{ cm}^{-2}$ and $N_d = 5 \times 10^{10} \text{ cm}^{-2}$.

while α varies strongly with z_i inside the well. For a fixed electron density the dependence of \tilde{N}_i , E_B , α , and β on the impurity location z_i is shown in Fig. 18 within the SPA and the RPA screening. We find that β is constant in this case and in QW's, see Fig. 10. We conclude that the variation of β with z_i found in Fig. 17 is due to the variation of the confinement in this case: $N = N_i$. We notice that due to the high electron density used in Fig. 18, \tilde{N}_i and E_B are strongly reduced in Fig. 18 in comparison to Fig. 16(b).

V. DISCUSSION AND COMPARISON WITH EXPERIMENTS AND OTHER THEORIES

In this section, we discuss our results and compare them with experimental and other theoretical results. Ground-state and excited-state levels of a single hydrogenic impurity have been widely investigated theoretically in QW's,¹⁻¹⁰ using variational wave-function methods. These results generally agree with experimental results on moderately doped samples.¹¹ In particular, the effects of the QW width, impurity position, barrier height, screening, and magnetic field are well accounted for by the theory.

For low-enough impurity concentrations, for which we find typically $N_i < 1 \times 10^9 \text{ cm}^{-2}$, using the full multiple-scattering calculations, we obtain an IB which is very close to the calculated single-impurity level for various carrier concentrations, impurity positions, and QW widths, see Figs. 4, 6, and 8. On the other hand, the separable potential approximation has proved to be a good approximation to calculate easily the binding energy in the low-impurity-density limit. The results are in agreement with Bastard's¹ calculations, see Fig. 8. As in Bastard's work, we have assumed infinite barrier height, even though a finite height could be included in our theory. Our main goal was to investigate the broadening and the shift of impurity levels as the impurity concentration increases. Notice that even for the low impurity concentrations, the IB width is not negligible. For instance, in case of $N = N_i = 1 \times 10^9 \text{ cm}^{-2}$, $L = 100 \text{ \AA}$, and $z_i = 50 \text{ \AA}$ (impurities in the middle of QW), the IB width is equal to $0.6R$ ($\approx 3 \text{ meV}$). The IB width decreases when the carrier concentration is increased; for example, in the above case with $N = 1 \times 10^{11} \text{ cm}^{-2}$ it amounts to $0.37R$ ($\approx 2 \text{ meV}$), see Figs. 3 and 4. The IB also shrinks as the impurities are moved away from the center of the QW, see Fig. 4, and as the QW width is increased, see Figs. 6 and 7. In all of these situations, the IB shrinkage is easily understood as the result of the weakening of the effective electron-impurity interaction.

Our multiple-scattering method is powerful enough to describe excited impurity bands for low impurity concentrations as well. It is worthwhile to notice that the energy ordering of impurity-band states, namely $1s$, $2p_{\pm}$, $2s$, and $2p_0$ is the same as that found within the single-impurity theories^{2,3,6-8} and observed experimentally.¹¹ Let us note that the shapes of the spectral densities of these states as a function of wave number are different according to their symmetry, see Figs. 12 and 13.

As the impurity concentration increases, the IB ground

state and excited states broaden and move toward the conduction subband. Due to this broadening and this shift, the excited states merge and gradually meet the conduction subband. For higher concentrations, the IB ground state also merges with the CSB to give a large band tail which extends into the energy gap as the impurity concentration is increased further. The spectral density analysis has allowed us to distinguish between extended states and quasiautomatic states. The latter are found to lie in the IB and in the lower-energy part of the BT. The contribution of the electron-impurity interaction to the gap shrinkage may be even larger than that of many-body effects, see Eq. (18) and Refs. 34–37. Notice that the factor α in Eq. (18) is obtained within the separable-potential approximation. The full calculations give a larger α as may be seen by looking at the data of Fig. 3. However, in Ref. 24 we have shown that the calculations of the gap shrinkage in the separable-potential approximation are in fair agreement with the full calculations. In this paper we did not calculate the gap shrinkage in the full approximation since we considered neither the electrostatic effects on the position of the bands, nor the effect of impurities on the valence subbands. The latter effect could be calculated as we have done it in the three-dimensional case.²⁸ On the other hand, the strength of the electron-impurity interaction is reflected in the values of the binding energy E_B and of the concentration \tilde{N}_i , for which the conduction and impurity bands meet. Both are increasing functions of the potential strength. We have shown that the ratio \tilde{N}_i/E_B is nearly constant.

Our present results have been obtained by using a RPA screened potential. It is well known that this potential is valid only when the screening is due to free electrons. It is less valid when the electrons are bound to impurities. This is the reason why the use of this potential allows us only a semiquantitative comparison with experimental results. We believe, however, that this potential provides a good description of IB electronic structure in the low concentration range because it has the right limit of the bare potential as $N \rightarrow 0$. On the other hand, the importance of multiple-occupancy corrections, which are mentioned in the Introduction, have not yet been estimated, to our knowledge, in the case of the finite-range potential.

In the light of our results, it would be interesting to study experimentally the transitions $1s \rightarrow 2p_{\pm}$, $1s \rightarrow$ continuum, etc., as functions of N_i and N in order to determine the onsets of merging of IB excited states and the ground state with the conduction subband. The latter should be accompanied by an insulator-to-metal transition that should be observable in low-temperature transport measurements for example.

It has been reported by Bastard *et al.*^{1,21} that a broadening of impurity levels is expected for a uniform doping in the well because the binding energy is strongly dependent on the position of the impurity. In this work, we have shown that another broadening mechanism exists due to the overlap of impurity wave functions as the concentration increases, even for a spike doping. We be-

lieve that the $1s$, $2p_{\pm}$, and $2s$ IB widths and energy shifts that we have calculated, see Fig. 11, may, on their own, explain the broadenings and energy shifts of the transitions lines observed in magnetoabsorption and electron Raman scattering¹¹ for concentrations comparable with those used in Fig. 11, without referring to any impurity migration in the well. Incidentally, it is worth mentioning that if the impurities are put intentionally in two different positions,³⁸ the resulting DOS is not merely the sum of the two DOS's, each one being considered separately. Indeed, as we have shown in the three-dimensional case²⁸ and in silicon inversion layers (see Ref. 24, Appendix), one has to replace the multiple-scattering equation for $U(k, q, E)$, see Eq. (6) in Ref. 24, by a set of two coupled equations for the two impurity positions, see Eq. (A3) in Ref. 24. The coupling comes from the electron Green function. Work on this issue is in progress.

We have also studied the electronic structure of selectively doped heterostructures as a function of the relevant parameters: depletion density, carrier and impurity concentrations, and the position of impurities. All we have said on QW's is also found in HS's. In particular, we have calculated the binding energy, the impurity concentration \tilde{N}_i for which the bands merge, the relation between two quantities, and the contribution of the electron-impurity interaction to the gap shrinkage. We did not succeed in finding enough results in the literature in order to compare them with ours.

VI. SUMMARY

To summarize, this work is aimed at generalizing the single-impurity studies of quantum wells and heterostructures and applying them to the case in which the impurity concentration is high enough for the single-impurity approximation to be no longer valid. Using a multiple-scattering method, we have succeeded in obtaining the impurity-band ground state and excited states and showed how these bands gradually merge with the lowest conduction subband as the impurity concentration is increased. This leads to the formation of a band tail.

Our method which is devised to study the many impurity scattering effects on the electronic structure is also a good approximation in the low-density limit, in agreement with single-impurity calculations. Thus it has proved to be a sound theory to study the effects of charged impurities on the electronic structure. Results on the QW width dependence of \tilde{N}_i , α , and β , see Eqs. (17) and (18), have been discussed in a brief report.³⁹

ACKNOWLEDGMENTS

We acknowledge stimulating discussions with F. Koch. One of the authors (A.G.) thanks the Ernst von Siemens Stipendium for financial support. The Groupe de Physique des Solides de l'Ecole Normale Supérieure is a Laboratoire associé au Centre National de la Recherche Scientifique.

- *Present address: Physik-Department (E16), Technische Universität München, D-8046 Garching bei München, Federal Republic of Germany.
- ¹G. Bastard, Phys. Rev. B **24**, 4714 (1981).
 - ²C. Mailhiot, Y.-C. Chang, and T. C. McGill, Phys. Rev. B **26**, 4449 (1982).
 - ³R. L. Greene and K. K. Bajaj, Solid State Commun. **45**, 825 (1983).
 - ⁴W.-M. Liu and J. J. Quinn, Phys. Rev. B **31**, 2348 (1985).
 - ⁵J. A. Brum, G. Bastard, and C. Guillemot, Phys. Rev. B **30**, 905 (1984).
 - ⁶R. L. Greene and K. K. Bajaj, Phys. Rev. B **31**, 4006 (1985).
 - ⁷K. Jayakumar, S. Balasubramanian, and M. Tomak, Phys. Rev. B **34**, 8794 (1986).
 - ⁸P. Lane and R. L. Greene, Phys. Rev. B **33**, 5871 (1986).
 - ⁹S. Chaudhuri and K. K. Bajaj, Solid State Commun. **52**, 967 (1984).
 - ¹⁰R. L. Greene and K. K. Bajaj, Phys. Rev. B **31**, 913 (1985).
 - ¹¹B. D. McCombe, N. C. Jarosik, and J.-M. Mercy, in *Two-Dimensional Systems: Physics and New Devices*, edited by G. Bauer, F. Kuchar, and H. Heinrich (Springer-Verlag, Berlin, 1986), p. 156; B. V. Shanabrook, Physica B+C **146B**, 121 (1987).
 - ¹²T. Ando, J. Phys. Soc. Jpn. **51**, 3900 (1982).
 - ¹³F. Stern, Appl. Phys. Lett. **43**, 974 (1983).
 - ¹⁴W. Walukiewicz, H. E. Ruda, J. Lagowski, and H. C. Gatos, Phys. Rev. B **30**, 4571 (1984).
 - ¹⁵S. Mori and T. Ando, J. Phys. Soc. Jpn. **48**, 865 (1980).
 - ¹⁶J. Lee, H. Spector, and V. Arora, J. Appl. Phys. **54**, 6995 (1983); H. Spector and V. Arora, Surf. Sci. **159**, 425 (1985).
 - ¹⁷G. Fishman and C. Calecki, Phys. Rev. B **29**, 5779 (1984).
 - ¹⁸F. Stern and W. Howard, Phys. Rev. **163**, 816 (1967).
 - ¹⁹A. Gold, Z. Phys. B **63**, 1 (1986); J. Phys. (Paris) Colloq. **48**, C5-255 (1987).
 - ²⁰A. Gold, Phys. Rev. B **35**, 723 (1987).
 - ²¹G. Bastard, E. E. Mendez, L. L. Chang, and L. Esaki, Solid State Commun. **45**, 367 (1983).
 - ²²M. Takeshima, Phys. Rev. B **33**, 4054 (1986); **34**, 1041 (1986).
 - ²³E. A. Andrada e Silva and I. C. da Cunha Lima, Solid State Commun. **64**, 113 (1987).
 - ²⁴A. Gold, J. Serre, and A. Ghazali, Phys. Rev. B **37**, 4589 (1988).
 - ²⁵A. Ghazali, A. Gold, and J. Serre, Surf. Sci. **196**, 346 (1988).
 - ²⁶G. Timp, A. B. Fowler, A. Hartstein, and P. N. Butcher, Phys. Rev. B **34**, 8771 (1986).
 - ²⁷J. R. Klauder, Ann. Phys. (N.Y.) **14**, 43 (1961).
 - ²⁸A. Ghazali and J. Serre, Phys. Rev. Lett. **48**, 886 (1982); J. Serre and A. Ghazali, Phys. Rev. B **28**, 4704 (1983).
 - ²⁹R. Schwabe, A. Haufe, V. Gottschalch, and K. Unger, Solid State Commun. **58**, 485 (1986).
 - ³⁰T. Ando, A. B. Fowler, and F. Stern, Rev. Mod. Phys. **54**, 437 (1982).
 - ³¹D. Pines and P. Nozières, *The Theory of Quantum Liquids*, (Benjamin, New York, 1966).
 - ³²J. Alvarez and F. Flores, J. Phys. F **15**, 2465 (1985).
 - ³³B. Vinter, Phys. Rev. B **13**, 4447 (1976).
 - ³⁴S. Schmitt-Rink, C. Ell, S. W. Koch, H. E. Schmidt, and H. Haug, Solid State Commun. **52**, 123 (1984).
 - ³⁵G. E. W. Bauer and T. Ando, Phys. Rev. B **31**, 8321 (1985).
 - ³⁶D. A. Kleinman and R. C. Miller, Phys. Rev. B **32**, 2266 (1985).
 - ³⁷C. Delalande, G. Bastard, J. Orgonasi, J. A. Brum, H. W. Liu, M. Voos, G. Weimann, and W. Schlapp, Phys. Rev. Lett. **59**, 2690 (1987).
 - ³⁸J.-M. Mercy, B. D. McCombe, W. Beard, J. Ralston, and G. Wicks, Surf. Sci. **196**, 334 (1988); D. Gammon, E. Glaser, B. V. Shanabrook, and D. Musser, *ibid.* **196**, 359 (1988); E. Glaser, B. V. Shanabrook, R. L. Hawkins, W. Beard, J.-M. Mercy, B. D. McCombe, and D. Musser, Phys. Rev. B **36**, 8185 (1987).
 - ³⁹A. Gold, J. Serre, and A. Ghazali, in Proceedings of the 19th International Conference on the Physics of Semiconductors, Warsaw, August, 1988 (to be published).